EDGEWOOD

CHEMICAL BIOLOGICAL CENTER

U.S. ARMY RESEARCH, DEVELOPMENT AND ENGINEERING COMMAND

ECBC-TR-828

TOXIC INDUSTRIAL CHEMICAL REMOVAL BY ISOSTRUCTURAL METAL-ORGANIC FRAMEWORKS

Gregory W. Peterson

RESEARCH AND TECHNOLOGY DIRECTORATE

T. Grant Glover
Bryan J. Schindler

SAIC
From Science to Solutions

SCIENCE APPLICATIONS
INTERNATIONAL CORPORATION
Gunpowder, MD 21010-0068

David Britt
Omar Yaghi

UNIVERSITY OF CALIFORNIA
Los Angeles, CA 90095-1569

January 2011

ABERDEEN PROVING GROUND, MD 21010-5424

Disclaimer

The findings in this report are not to be construed as an official Department of the Army position unless so designated by other authorizing documents.

REPORT DOCUMENTATION PAGE

Form Approved
OMB No. 0704-0188

1. REPORT DATE *(DD-MM-YYYY)*	2. REPORT TYPE	3. DATES COVERED *(From – To)*
XX-01-2011	Final	Feb 2008 - Mar 2009

4. TITLE AND SUBTITLE
Toxic Industrial Chemical Removal by Isostructural Metal-Organic Frameworks

5a. CONTRACT NUMBER

5b. GRANT NUMBER

5c. PROGRAM ELEMENT NUMBER

6. AUTHOR(S)
Peterson, Gregory W. (ECBC); Glover, T. Grant; Schindler, Bryan J. (SAIC); Britt, David; and Yaghi, Omar (UCLA)

5d. PROJECT NUMBER
BA07PRO104

5e. TASK NUMBER

5f. WORK UNIT NUMBER

7. PERFORMING ORGANIZATION NAME(S) AND ADDRESS(ES)
DIR, ECBC, ATTN: RDCB-DRP-F, APG, MD 21010-5424
SAIC, Inc., P.O. Box 68, Gunpowder, MD 21010-0068
UCLA, Department of Chemistry and Biochemistry, 607 Charles E. Young Drive East, Box 951569, Los Angeles, CA 90095-1569

8. PERFORMING ORGANIZATION REPORT NUMBER
ECBC-TR-828

9. SPONSORING / MONITORING AGENCY NAME(S) AND ADDRESS(ES)
Joint Science and Technology Office - Chemical and Biological Defense, Defense Threat Reduction Agency, John J. Kingman Road, Fort Belvoir, VA 22060-6201

10. SPONSOR/MONITOR'S ACRONYM(S)
JSTO-CBD, DTRA

11. SPONSOR/MONITOR'S REPORT NUMBER(S)

12. DISTRIBUTION / AVAILABILITY STATEMENT
Approved for public release; distribution is unlimited.

13. SUPPLEMENTARY NOTES

14. ABSTRACT

Cobalt, magnesium nickel, and zinc MOF-74 analogs have been synthesized, characterized, and evaluated as novel adsorbent materials for the removal of toxic industrial chemicals. Nitrogen porosity, X-ray diffraction, and water adsorption data are presented in addition to breakthrough curves for ammonia, octane, cyanogen chloride, and sulfur dioxide. The materials were evaluated in humid and dry conditions. The results show that in an isostructural environment changes in the metal contained in the structural building unit of MOF-74 materials have a significant effect on the resulting dynamic breakthrough capacity. In general, cobalt and magnesium MOF-74 materials perform better than either nickel or zinc MOF-74 in dry and humid conditions; however, in most cases, humidity significantly decreases the performance of all the materials studied.

15. SUBJECT TERMS

Metal-organic framework	MOF	MOF-74
Toxic industrial chemicals	TIC	Isostructural MOF

16. SECURITY CLASSIFICATION OF:			17. LIMITATION OF ABSTRACT	18. NUMBER OF PAGES	19a. NAME OF RESPONSIBLE PERSON
a. REPORT	b. ABSTRACT	c. THIS PAGE			Sandra J. Johnson
U	U	U	UL	34	19b. TELEPHONE NUMBER *(include area code)* (410) 436-2914

Blank

PREFACE

The work described in this report was authorized under DTRA Project No. BA07PRO104. This work was started in February 2008 and completed in March 2009.

The use of either trade or manufacturers' names in this report does not constitute an official endorsement of any commercial products. This report may not be cited for purposes of advertisement.

This report has been approved for public release. Registered users should request additional copies from the Defense Technical Information Center. Unregistered users should direct such requests to the National Technical Information Service.

Acknowledgments

The authors thank Amedeo Napolitano and Paulette Jones (SAIC, Gunpowder, MD), and Tara Sewell and John Mahle (U.S. Army Edgewood Chemical Biological Center) for evaluating these materials and gathering experimental data discussed in this report.

Blank

CONTENTS

FIGURES

TABLES

Blank

TOXIC INDUSTRIAL CHEMICAL REMOVAL BY ISOSTRUCTURAL METAL-ORGANIC FRAMEWORKS

1. INTRODUCTION

Metal-organic frameworks (MOFs) are a relatively new class of porous materials that are gaining wide interest for industrial processes such as gas storage, separations, and catalysis [1-4]. MOFs self-assemble using combinations of metal clusters and organic linking units. The vast number of combinations allow for unprecedented abilities to tune pore size and functionality on the molecular level, resulting in structures that can be modified for specific applications.

A variety of studies have been conducted on modifying the structural building units (SBUs) and organic linkers to achieve better selectivity and activity towards chemicals such as, hydrogen, carbon dioxide, and methane, for gas storage applications [5-6]. Relatively few studies, however, have looked at varying these structural components to remove toxic industrial chemicals (TICs) in dynamic situations [7-10].

Of the MOFs that have currently been reported in the literature, MOF-74, which is comprised of 1-dimensional hexagonal channels and is constructed from a 3-dimensional helical metal oxide rod SBU, is of particular interest [11]. The metal contained in the SBU of MOF-74 is typically cobalt (Co), magnesium (Mg), zinc (Zn), or nickel (Ni), and they are organized in the structure such that they are coordinately unsaturated, which may provide a means of performing chemical reactions in the pores of the material. The SBU, linker, and MOF-74 structure is illustrated in Figure 1.

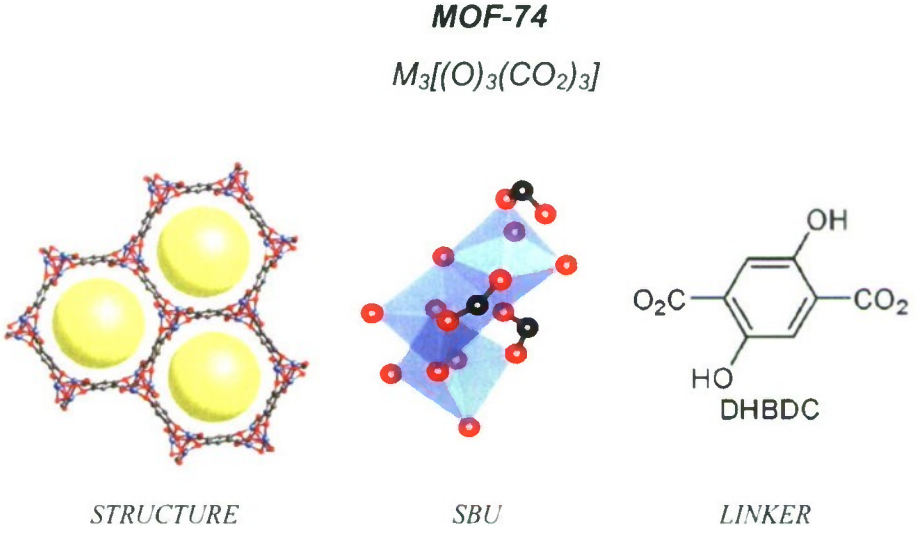

Figure 1. MOF-74 structural components [5,11]

Investigations have been conducted to determine how the metal in the SBU of MOF-74 impacts gas adsorption behavior. For example, Yildirim et al. found that hydrogen binding in isostructural MOFs correlated with the metal contained in the SBU. Binding energy was shown to follow the trend zinc<magnesium<cobalt<nickel [12]. The authors suggest that metal-hydrogen binding strength can be predicted using the empirical transition metal ion radius and the calculated distance between the MOF-74 metal and the adsorbed hydrogen molecule. In addition, the authors studied the methane storage capabilities of these MOFs and found that excess adsorption of methane correlated to the metal contained in the SBU and followed the trend magnesium<zinc<cobalt<nickel [13]. Carbon dioxide adsorption has also been correlated to the type of metal in the SBU of MOF-74 with zinc providing the least uptake, magnesium the greatest uptake, and cobalt and nickel providing similar loadings [14].

Several other fundamental aspects of MOF-74 have also been investigated. For example, Vitillo et al.[15] investigated the role of unsaturated metals in hydrogen adsorption. The hydrogen isotherms on MOF-5, nickel MOF-74, and MOF-199 were investigated; of these materials, nickel MOF-74 had the highest hydrogen uptake at low pressures, followed by MOF-199 and then MOF-5. Unsaturated metals have a large role in hydrogen adsorption, but the effect diminishes at high pressures where surface area and pore volume dominate.

In addition, Liu et al. examined the location of hydrogen adsorption in MOF-74 by performing a density functional theory calculation [16]. The simulations revealed that hydrogen binds first at the metal followed by adsorption near clusters of oxygen atoms, adsorption on the benzene structures, and finally with multilayer adsorbtion in the pore.

Although there appears to be a strong connection between the type of metal in the SBU and gas storage, little work has been done to investigate the relationship between SBU selection and dynamic air filtration. Therefore, the objectives of this report are to investigate the impact of different metals in the SBU for MOF-74 under dynamic filtration situations and to determine the capability of MOF-74 materials to purify air.

A variety of TICs are studied via fixed-bed breakthrough experiments to determine the effect of metal-type on a broad spectrum of chemistries. The chemicals studied in this report include ammonia, octane, cyanogen chloride (CK), and sulfur dioxide. From a filtration perspective, most of the TICs boil at a relatively low temperature and have high vapor pressures. In addition, ammonia is typically viewed as either a basic or base-forming gas; whereas, CK and sulfur dioxide are seen as either acidic or acid-forming gases, with CK considered a design-limiting chemical. Also, typically, sulfur dioxide is removed via oxidation; whereas, cyanogen chloride is removed by hydrolysis when these materials are filtered using metal impregnated carbons. Octane provides a basis to determine the physical adsorption capacity for other high boiling point toxic chemicals. Each of these chemicals provides a broad range of testing conditions upon which to assess the impact of specific metal building units in MOF-74.

2. EXPERIMENTATION

2.1 Synthesis of MOF-74 Analogs

2.1.1 Cobalt MOF-74 (Co-MOF-74)

2,5-Dihydroxyterephthalic acid (DHTA) (0.5 g) and $Co(NO_3)_2 \cdot 6H_2O$ (1.5 g) were dissolved in 70 mL dimethylformamide (DMF), 70 mL ethanol, and 70 mL water with sonication in a 400 mL jar. The jar was capped tightly and placed in a 100 °C oven for 2.75 days. After cooling to room temperature, the mother liquor was decanted, and the products were washed with and immersed in methanol. The methanol solvent was decanted and replaced once per day over the next 3 days. The products were then evacuated to dryness and heated under vacuum to 250 °C. After 24 hr, the sample was cooled to room temperature and stored.

2.1.2 Magnesium-MOF-74 (Mg-MOF-74)

DHTA (0.112 g) and $Mg(NO_3)_2 \cdot 6H_2O$ (0.475 g) were dissolved in 45 mL DMF, 3 mL ethanol, and 3 mL water with sonication. The solution was decanted into five 20 mL vials, which were capped tightly and placed in a 125 °C oven for 21 hr. After cooling to room temperature, the mother liquor was decanted and replaced with methanol. The products were combined into one batch, and the methanol solvent was decanted and replaced five times over the next 2 days. The sample was evacuated to dryness and heated under vacuum to 250 °C. After 6 hr, the samples was cooled to room temperature and stored.

2.1.3 Nickel-MOF-74 (Ni-MOF-74)

DHTA (0.5 g) and $Ni(NO_3)_2 \cdot 6H_2O$ (1.5 g) were dissolved in 70 mL DMF, 70 mL ethanol, and 70 mL water with sonication in a 400 mL jar. The jar was capped tightly and placed in a 100 °C oven for 2.75 days. After cooling to room temperature, the mother liquor was decanted, and the products were washed three times with DMF, three times with methanol, and immersed in methanol. The methanol solvent was decanted and replaced once per day over the next 3 days. The products were then evacuated to dryness and heated under vacuum to 250 °C. After 5 hr, the sample was cooled to room temperature and stored.

2.1.4 Zinc-MOF-74 (Zn-MOF-74)

DHTA (1.00 g) and $Zn(NO_3)_2 \cdot 4H_2O$ (4.52 g) were dissolved in 100 mL DMF in a 400 mL jar with sonication. Water (5 mL) was added, with more sonication. The jar was capped tightly and placed in a 110 °C oven for 21.5 hr. After cooling to room temperature, the mother liquor was decanted, and the products were washed three times with DMF, three times with methanol, and immersed in methanol. The methanol solvent was decanted and replaced once per day over the next 3 days. The products were then evacuated to dryness and heated under vacuum to 150 °C for 1 hr. After 10 hr at 150 °C, the heat was increased to 265 °C for 1 hr. After 10 hr at 265 °C, the sample was cooled to room temperature and stored.

2.2 Characterization

2.2.1 Powder X-ray Diffraction (PXRD)

PXRD data were collected using a Bruker D8-Discover θ-2θ diffractometer in reflectance Bragg-Brentano geometry using Ni filtered Cu Kα line focused radiation at 1600 W (40 kV, 40 mA) power and equipped with a Vantec Line detector. Radiation was focused using parallel focusing Gobel mirrors. The system was also outfitted with an anti-scattering shield, which prevents incident diffuse radiation from hitting the detector, eliminating the normally observed large background at $2\theta < 3^{\circ}$. Samples were mounted on glass slides by dropping powders from a wide-blade spatula and then leveling the sample surface with a spatula. Given that the particle size of the 'as synthesized' samples were already found to be quite mono-disperse, neither sample grinding nor sieving was used prior to analysis. We note, however, that the micron sized crystallites lead to peak broadening. The best counting statistics were achieved by collecting samples using a 0.02° 2θ step scan from 1.5 - 60° with an exposure time of 10 s per step. No peaks could be resolved from the baseline for $2\theta > 35^{\circ}$; therefore, this region was not considered for further analysis.

2.2.2 Adsorption Equilibrium

Cryogenic nitrogen isotherm data were collected with a Quantachrome Autosorb Automated Gas Sorption System. Nitrogen isotherm data were used to estimate the surface area and pore volume of the materials.

Water isotherms at 25 °C were collected using a Cahn microbalance as shown in Figure 2. Water was delivered from a saturator cell to a temperature-controlled Cahn balance containing the sorbent to be evaluated. The relative humidity (RH) was controlled by adjusting the temperature of the adsorption cell. The equilibrium loading was calculated from the change in the weight recorded by the Cahn microbalance.

2.2.3 Micro-Breakthrough Experiments

Analyte was injected into a ballast and subsequently pressurized; this chemical mixture was then mixed with an air stream containing the required moisture content to achieve a predetermined concentration. The completely mixed stream then passed through a sorbent bed submerged in a temperature-controlled water bath. The sorbent bed is filled on a volumetric basis in a 4 mm internal diameter tube to a height of 4 mm, resulting in approximately 20 mg of MOF-74 material being used for each test. The samples were regenerated in dry air at 120 °C for 1 hr, and humid samples were prehumidified in air at 80% RH at 20 °C for 2 hr. After saturating the sample, clean air was then passed to the sample, with the humidity of the clean air matching the conditions of the experiment, to evaluate the desorption behavior of the material. The dry air used in these experiments had a dew point of approximately -35 °C. In all cases, the effluent stream then passed through a continuously operating HP5890 Series II Gas Chromatograph A.

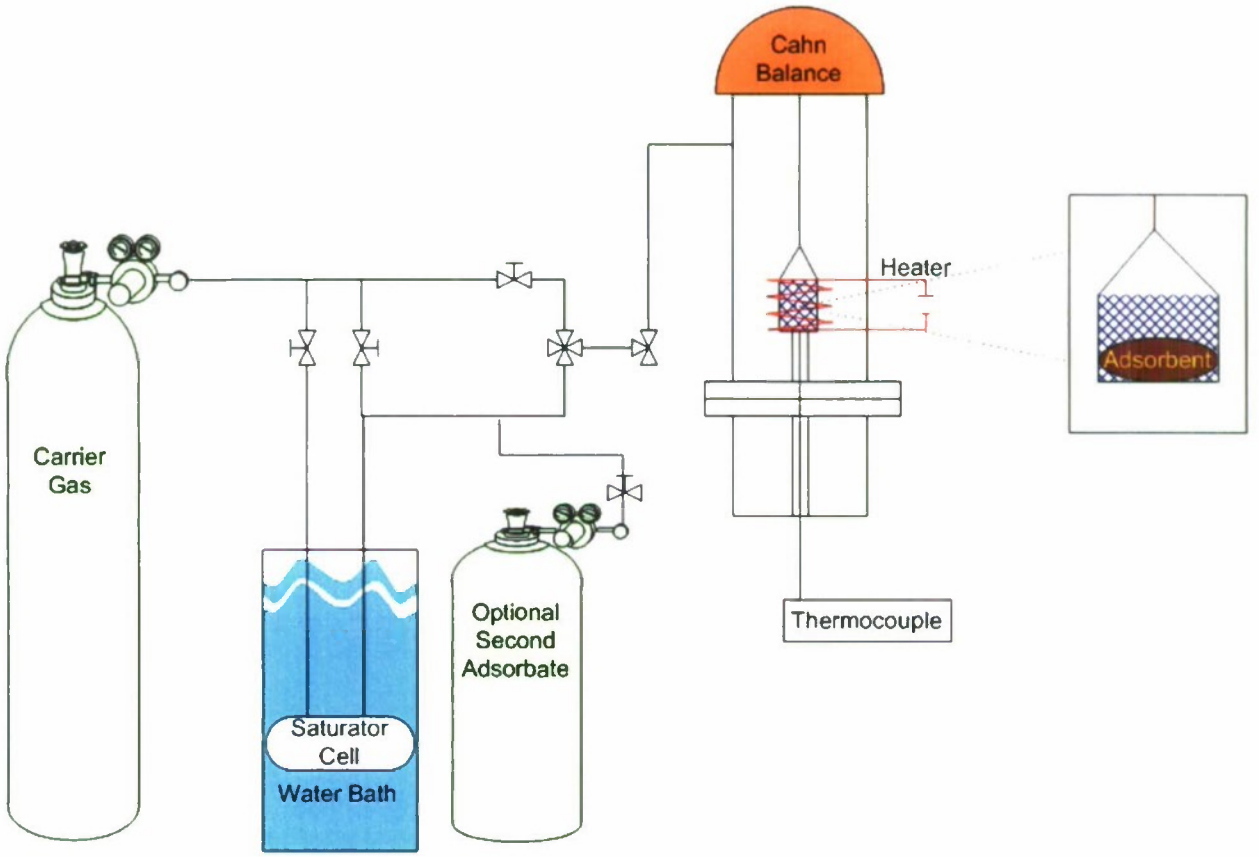

Figure 2. Water adsorption isotherm system

To establish a basis for the consisteney of the breakthrough deviee, control breakthrough experiments were performed using dry ammonia and an adsorbent similar to H-ZSM-5. Fifteen control runs were performed over 8 months using approximately 35 mg of adsorbent and bead height of approximately 4 mm. The average loading of all these tests was 2.2 mols/kg with a standard deviation of 0.2 mols/kg. These controls runs provide a high degree of confidenee in the repeatability of the breakthrough tests performed on the MOF-74 analogs.

All materials were stored in air prior to use. In most cases, breakthrough tests were run within the same month of synthesis of the MOF material. For the zine analog, the testing was spread out over 8 months after materials synthesis. For the magnesium analog, most breakthrough testing was eompleted within a month of the synthesis of the material. However, beeause Mg-MOF-74 is generally synthesized in limited quantities, it was neeessary for two additional samples to be synthesized and used for testing. Speeifieally, all magnesium analog tests were performed with the same sample exeept for the humid ammonia and humid oetane. A third sample was used to test humid sulfur dioxide. Although it would be preferred to test all of the materials using the same bateh of sorbent, this was not possible due to limited amounts of material and the extensive number of tests performed in this study. Magnesium was the only analog that required multiple batehes to eomplete the testing. All batehes of the magnesium

analog had similar physical properties in regards to surface area and porosity. A system schematic is shown in Figure 3.

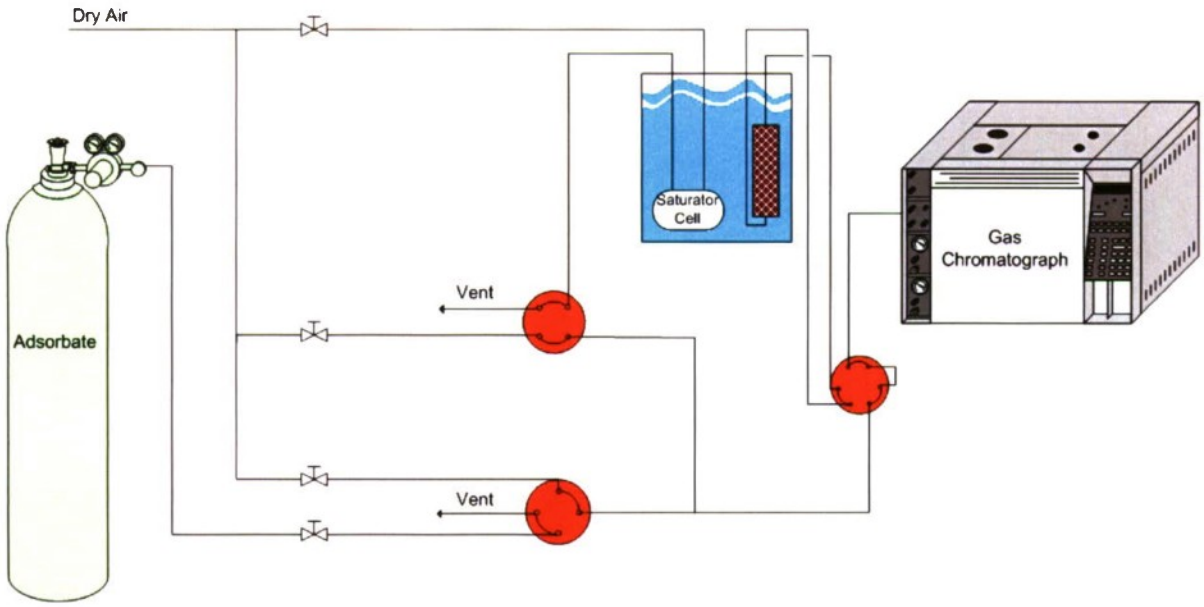

Figure 3. Rapid nanoporous adsorbent breakthrough testing apparatus

2.2.3.1 Ammonia

Approximately 50 mm^3 of sorbent were evaluated using an ammonia challenge at a feed concentration of 1000 mg/m^3 in air, a flow rate of 20 mL/min referenced to 20 °C, and RH of approximately 0% and 80%. The residence time (bed volume divided by the flow rate) was approximately 0.15 s. The effluent concentrations were monitored using a photoionization detector (PID).

2.2.3.2 Cyanogen Chloride

Approximately 50 mm^3 of sorbent were evaluated using a cyanogen chloride (ClCN or CK) challenge at a feed concentration of 4,000 mg/m^3 in air, a flow rate of 20 mL/min referenced to 20 °C, and RH of approximately 0% and 80%. The residence time (bed volume divided by the flow rate) was approximately 0.15 s. The effluent concentrations were monitored using a flame ionization detector (FID).

2.2.3.3 Octane

Approximately 50 mm^3 of sorbent were evaluated using an octane challenge at a feed concentration of 4,000 mg/m^3 in air, a flow rate of 20 mL/min referenced to 20 °C, and RH of approximately 0% and 80%. The effluent concentrations were monitored with a FID.

2.2.3.4 Sulfur Dioxide

Approximately 50 mm^3 of sorbent were evaluated with sulfur dioxide at a feed concentration of 1,000 mg/m^3, a flow rate of 20 mL/min referenced to 20 °C, and RH of approximately 0% and 80%. The concentration eluting through the sorbent was monitored with a flame photometric detector (FPD).

3. THEORY

Breakthrough data were used to calculate the dynamic capacity to saturation using the following equations. First, a concentration-time, or Ct, number is defined as:

$$Ct_{feed} = t_f C_{feed} \tag{1}$$

where Ct_{feed} has units of mg-min/m^3, t_f is the time that the feed is passed to the system, and C_{feed} is the concentration of the feed in mg/m^3.

The Ct eluting from the sorbent until feed termination is calculated by integrating under the elution curve using the mid-point rule:

$$Ct_{elution} = \sum_{t=0}^{ts} \frac{C_n + C_{n-1}}{2}\left(t_{n-1} - t_n\right) \tag{2}$$

where $Ct_{elution}$ has units of mg-min/m^3, t_s is the time to saturation in minutes, Ct_n is the concentration at time n in mg/m^3, and Ct_{n-1} is the concentration at time n-1 in mg/m^3.

Equation 2 is also used when accounting for either desorption or the amount of chemical off-gassing from the sorbent after feed termination. Equation 3 is used to calculate W_E, the effective loading to saturation, with and without desorption:

$$W_E = \frac{\left(Ct_{Feed} - Ct_{Elution} - Ct_{Desorption}\right)F_{feed}}{M_{ads} MW} 10^{-6} \tag{3}$$

where M_{ads} is the mass of the adsorbent in mg, MW is the molecular weight of the chemical in the feed in mg/mol, F_{feed} is the feed flow rate in m^3/min, and W_E has units of mol/kg.

Application of these equations assumes that any analyte that resides downstream of the bed after breakthrough is quickly purged from the system without any effective tailing, and all tailing is attributed to desorption of adsorbate from the porous material. Experimentally, it is assumed that any gas downstream of the bead is quickly swept away as a result of the large flow rate (20 mL/min) relative to the small tubing diameter (1/16 in.).

4. RESULTS AND DISCUSSION

After synthesis, the crystal structure of MOF-74 was verified via PXRD, and the results are shown in Figure 4.

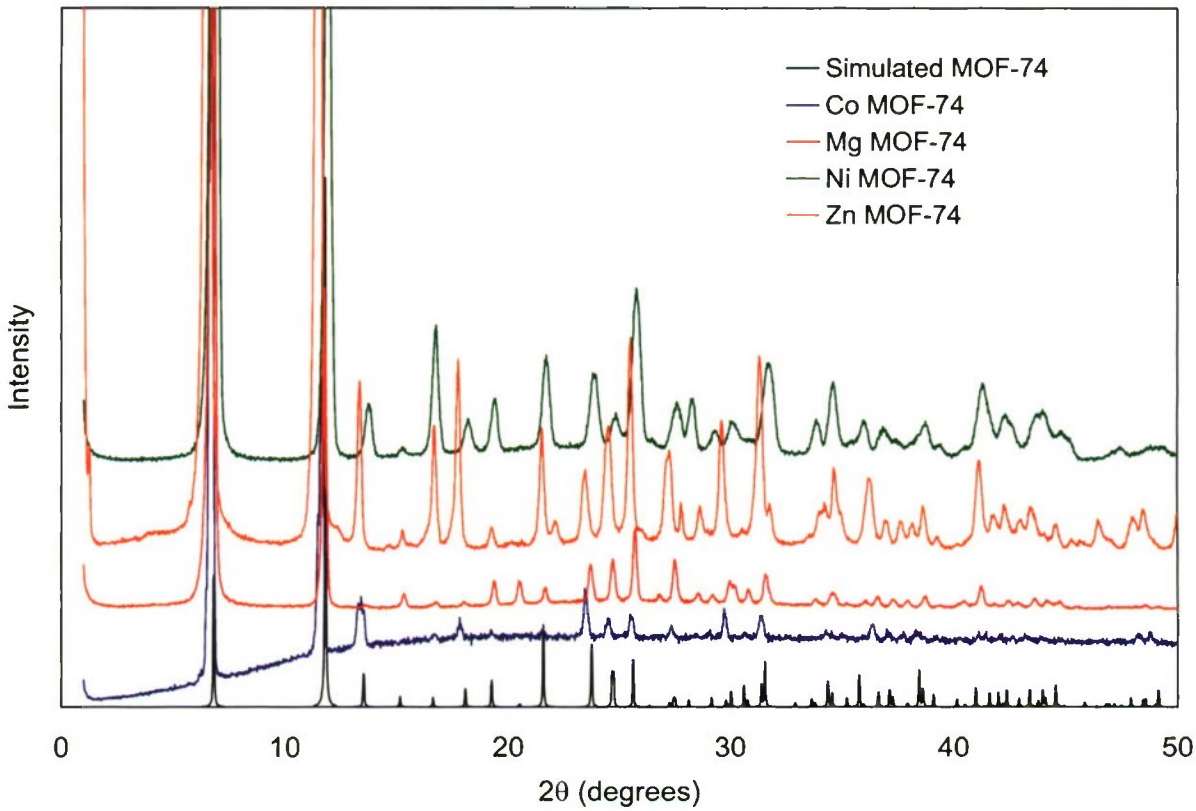

Figure 4. Powder X-Ray diffraction patterns for MOF-74 analogs

The PXRD patterns for all of these materials match the theoretical pattern. The low angle peaks agree for all synthesized materials compared to the theoretical MOF-74, indicating that the long range order of the materials is consistent. High angle peaks of all the samples are consistent with the theoretical MOF-74 pattern. The zinc and nickel samples show the closest match to the theoretical XRD pattern, indicating that the structures are nearly identical.

The nitrogen adsorption isotherms at 77 K shown in Figure 5 are consistent with highly porous materials, indicating that these materials have been sufficiently activated. The BET surface area, the theoretical surface area as calculated from the crystal structure, and the pore volume of the materials are listed in Table 1.

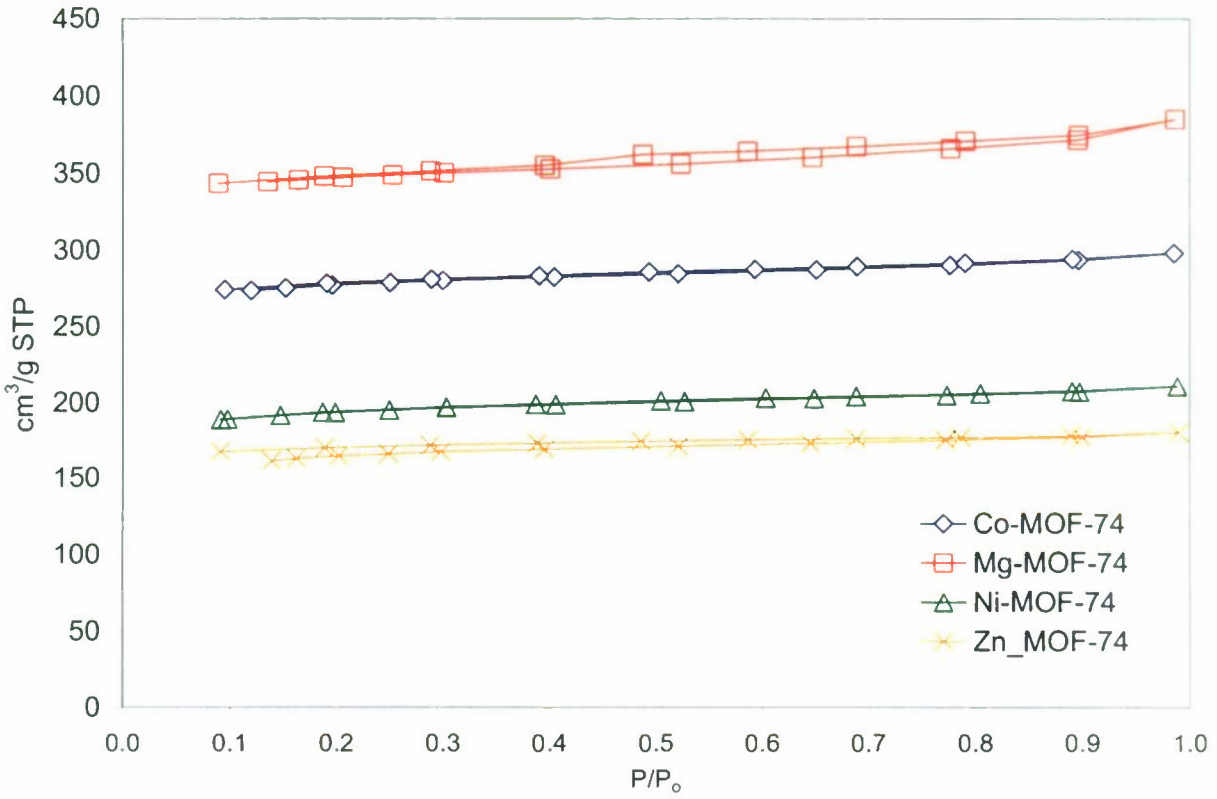

Figure 5. Nitrogen adsorption isotherms for various MOF-74 materials

Table 1. BET Capacities of MOF-74 Analogs

MOF-74 Analog	BET Area	Theoretical BET Area
	m^2/g-adsorbent	m^2/g-adsorbent
Mg-MOF-74	1206	2517
Co-MOF-74	835	1958
Ni-MOF-74	599	1961
Zn-MOF-74	496	1880

The surface areas reported in Table 1 show that the MOF materials are still significantly under activated when compared to the theoretical areas of the material. However, the results for the surface area of these MOF-74 samples are consistent with the surface areas reported by others [14].

Examining the surface area of MOF-74 presents a unique opportunity to study the impact of metals in an isostructural environment. For example, Caskey et al. [14] note that because surface area is reported on a per gram basis, the mass of the metals in the MOF-74 structure directly contributes to the resulting BET area. In their work, the BET surface areas for their MOF-74 samples are consistent with heaver metals resulting in lower surface areas. For

example, the BET area of Mg-MOF-74 reported in their work is 1495 m^2/g with Co-MOF-74 having less surface area (1080 m^2/g), followed by Ni-MOF-74 (1070 m^2/g), and Zn-MOF-74 (816 m^2/g). Caskey et al. further illustrate the idea by examining the adsorption of nitrogen in molecules per unit cell. The authors note that 35-38 nitrogen molecules per unit cell occupy the material regardless of the metal contained in the SBU.

Because the TIC filtration experiments will be conducted in dry and humid conditions, water adsorption isotherms for the MOF-74 samples were measured. Water is of particular interest because it is common for water to compete with adsorption sites in nanoporous materials and reduce the capacity of the adsorbent for the targeted chemical of interest. Water also co-adsorbs with some chemicals and increases the capacity of other materials, but the phenomena is complex and depends on the nature of the adsorbent and the adsorbate [17-19]. Water adsorption is particularly important in regards to air purification, given the natural humidity of ambient air. The water adsorption isotherms for MOF-74 are shown in Figure 6.

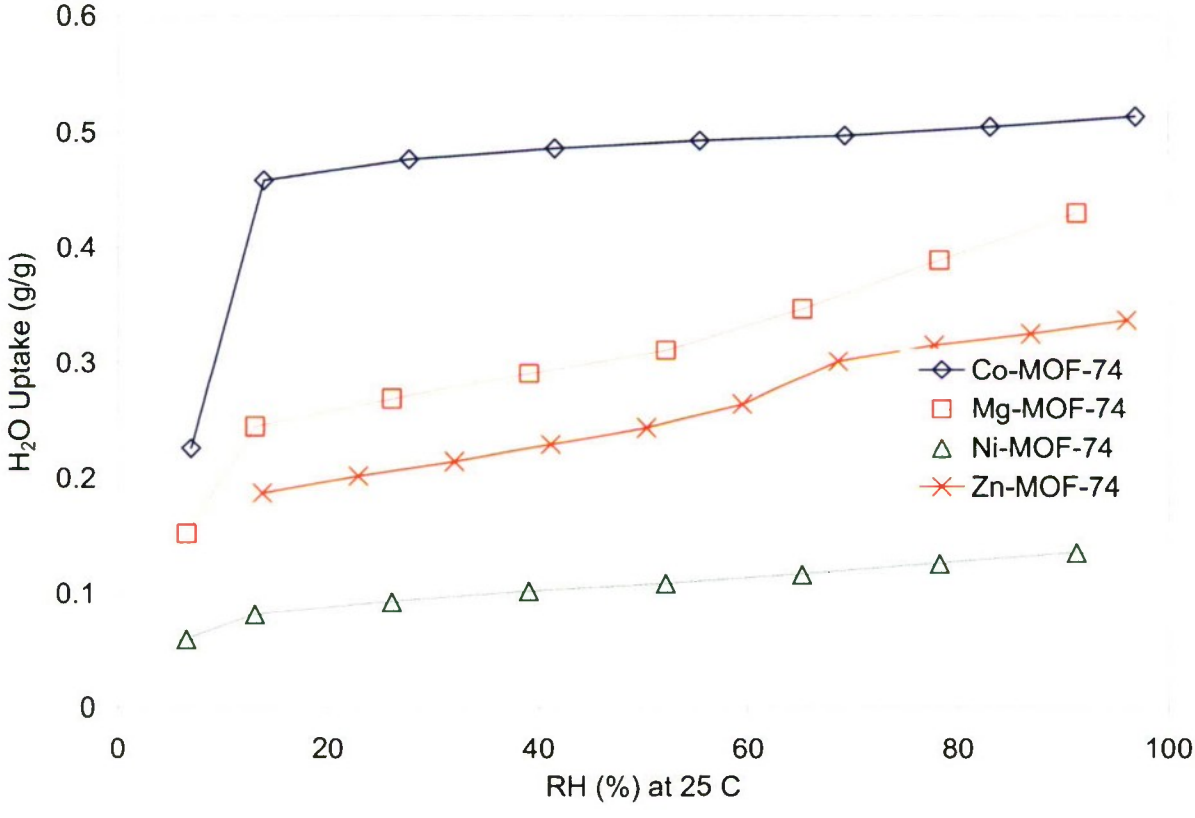

Figure 6. Water adsorption equilibria at 25 °C for MOF-74

Water isotherm data show that the cobalt analog adsorbs the most moisture over the entire range of RH conditions studied, and saturates at very low RH conditions. Due to the open metal sites, water loads on the samples considerably with the saturation capacity of cobalt and magnesium MOF-74 being close to that of activated carbon [19].

After these materials were synthesized, they were stored in a nitrogen environment prior to performing the BET surface area and PXRD analysis. After verifying the structure and porosity of the materials, they were subsequently stored in air under ambient moisture conditions. Therefore, the sensitivity of these materials to ambient conditions is also reflected in these isotherms. Specifically, if a MOF analog loses its structural order upon exposure to air, then any isotherms measured after that exposure may reflect lower loading than a material stored under dry conditions. Table 2 summarizes the moisture loadings at three RH conditions.

Table 2. Water Loading of Sorbents at 25 °C

MOF-74 Analog	Water Loading (g-water/g-sorbent)		
	15% RH	50% RH	80% RH
Co	0.46	0.49	0.50
Mg	0.25	0.31	0.39
Ni	0.08	0.11	0.13
Zn	0.19	0.24	0.32

4.1 Breakthrough Results

4.1.1 Ammonia

Ammonia micro-breakthrough testing was conducted on MOF samples under dry and humid conditions to assess ammonia reactive capacity and, more generally, the potential of MOF-74 analogs to filter basic gases. Ammonia breakthrough curves under dry RH conditions are illustrated in Figure 7. In this figure, the time for each sample has been normalized per gram of adsorbent used in the test. The volume for each of these tests is the same, but the mass varies; therefore, to compare the breakthrough times, it is necessary to correct for the difference in sample mass used for each experiment.

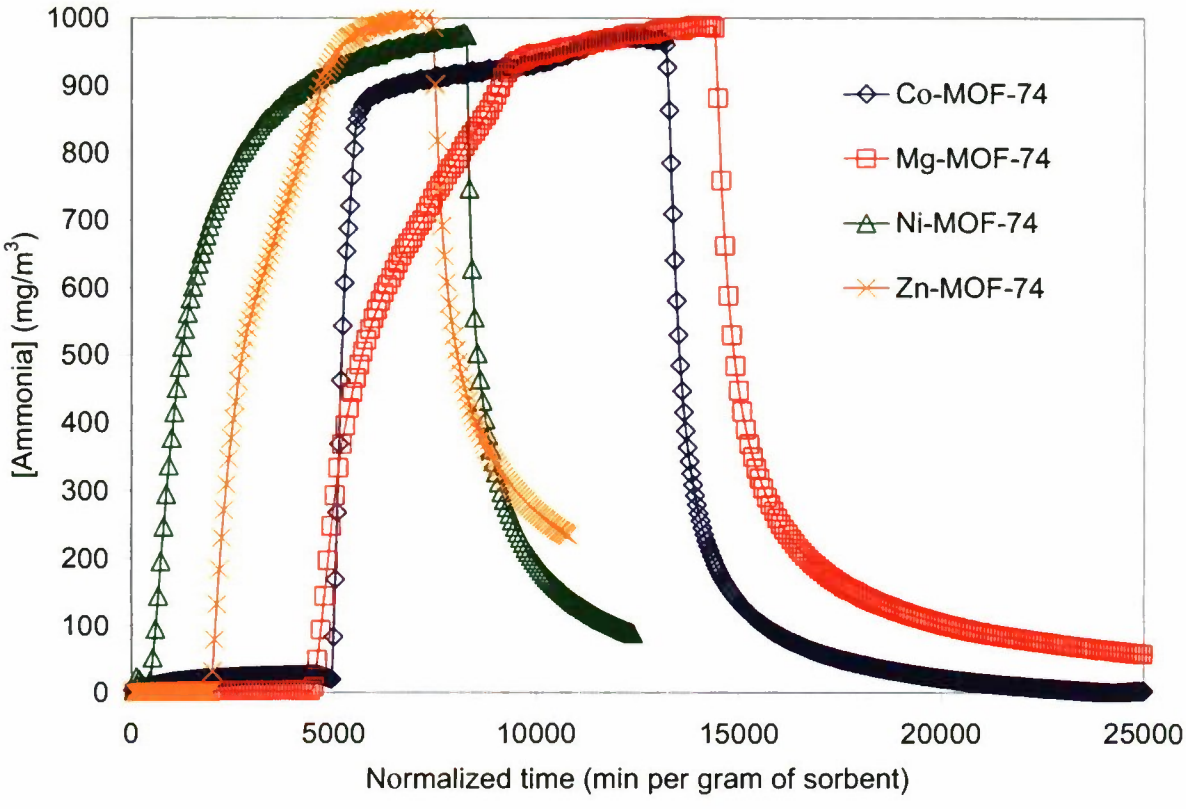

Figure 7. Ammonia breakthrough curves under dry (RH = 0%) conditions

Results indicate that the cobalt and magnesium analogs both provide substantial ammonia filtration capabilities. The Ni-MOF-74 analog exhibits some filtration capacity along with the Zn-MOF-74 material.

After saturation, the feed gas is changed to clean air to determine the capability of the material to retain the adsorbed gas. The clean air used for desorption has the same RH as the testing condition. In the ideal case, the adsorbate would be retained irreversibly; as the clean air passes through the system, nothing would be eluted from the bed. This type of behavior would result in the desorption portion of the breakthrough curve that would be vertical.

In the case above, some desorption is present indicating weakly physisorbed ammonia in the pores of all the MOF-74 analogs. The physisorb ammonia, which fills the MOF pore, likely experiences little interaction with the active metal adsorption site in the SBU and is more readily desorbed from the material. The cobalt and magnesium analogs retain 83 and 70% of the ammonia, respectively, indicating that the ammonia is more strongly bound to these analogs than the zinc and nickel MOFs.

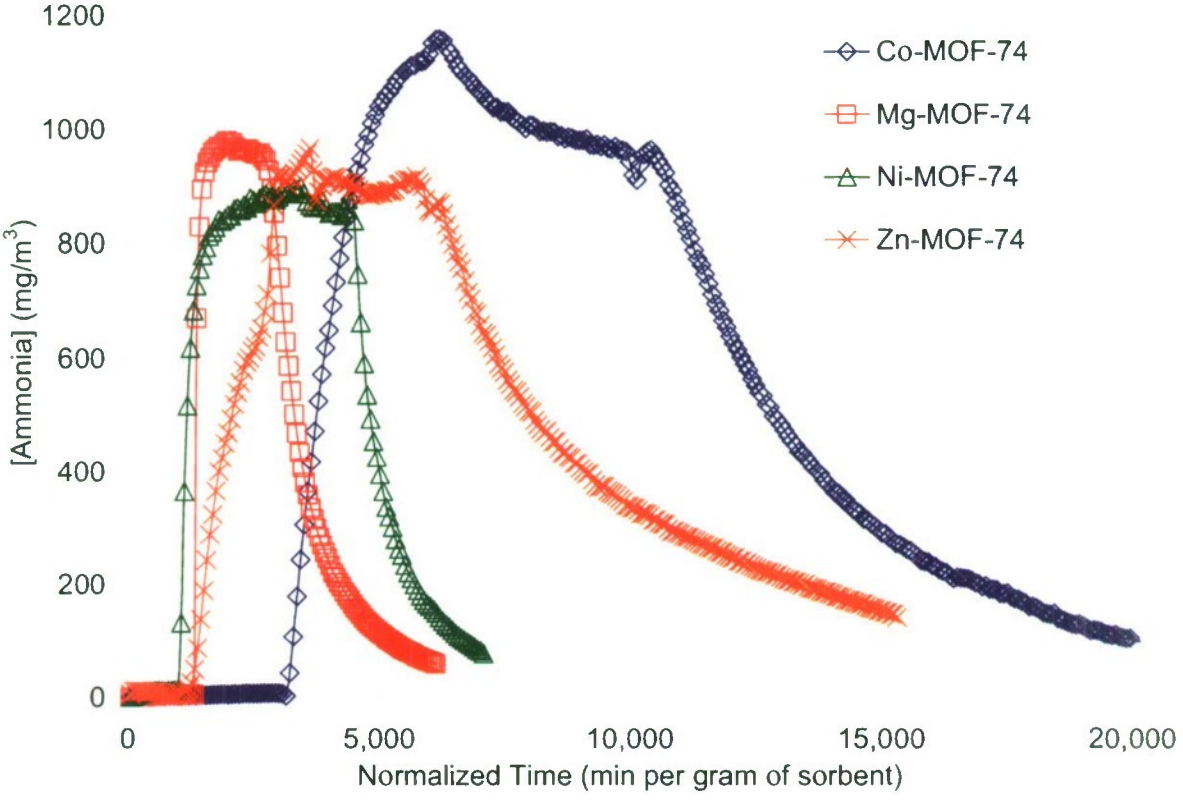

Figure 8. Ammonia breakthrough curves under humid (RH = 80%) conditions

Ammonia breakthrough curves under humid (80% RH) conditions are illustrated in Figure 8. This figure shows that the cobalt analog continues to outperform the other MOF-74 analogs in a humid environment. However, all the MOF materials show a reduction in capacity when filtering ammonia from a humid air stream. The cobalt, zinc, and magnesium analogs show a significant amount of ammonia desorption as the clean humid air passes through the bed. The nickel analog, however, retains 60% of the adsorbed ammonia after desorption.

One possible explanation of the decrease in ammonia capacity in humid environments is that water is competing for the adsorption sites in the material, and that the prehumidification of the sample results in the active sites of the material being inaccessible to ammonia. However, the solubility of ammonia in water probably contributes to maintaining some dynamic capacity under humid conditions. The long tailing seen during the desorption could result from weakly bound ammonia being desorbed from the MOF-74 surface as water continues to load the material. A summary of the adsorption results is presented in Table 3.

Table 3. Ammonia Dynamic Capacity of Sorbents

MOF-74 Analog	Sorbent Mass*	Effective Loading	Effective Loading (w/Desorption)
	g	mol/kg	mol/kg
Co (Dry)	0.0233	6.660	5.540
Co (Wet)	0.0149	4.270	0.000
Mg (Dry)	0.0123	7.620	5.350
Mg (Wet)	0.0193	1.670	0.550
Ni (Dry)	0.0161	2.260	1.180
Ni (Wet)	0.0170	1.920	1.130
Zn (Dry)	0.0182	3.700	2.170
Zn (Wet)	0.0176	2.840	0.000

*Dry basis - does not include mass of loaded water

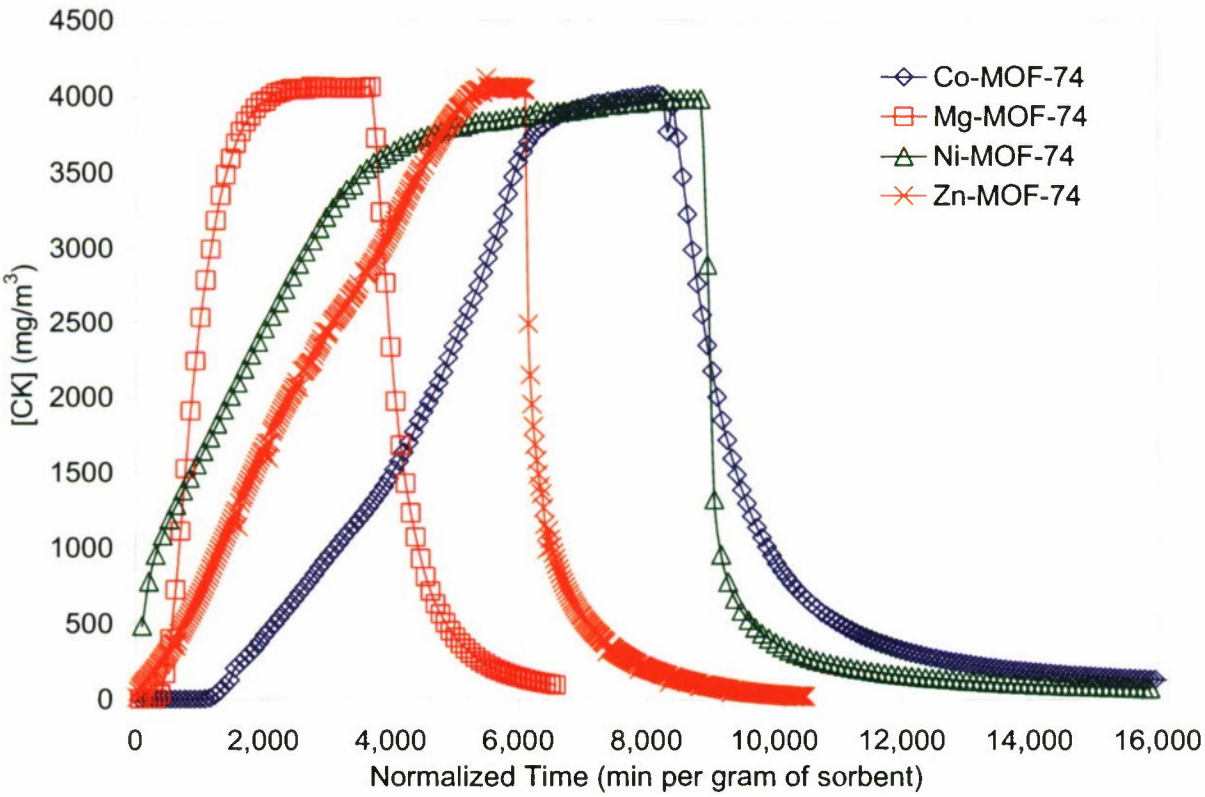

Figure 9. CK breakthrough curves under low-RH conditions

4.1.2 Cyanogen Chloride

CK miero-breakthrough testing was also eondueted to evaluate the potential of MOF-74 analogs to remove aeid forming gases.

It is elear from the data shown in Figure 9 that the eobalt, zine, and nickel materials all provide noteworthy filtration capaeity for dry CK. In all three cases, the likely meehanism of removal is CK eoordination with the open metal sites. However, it is diffieult to determine precisely how CK adsorbs on the surface of MOF-74 and how those meehanisms in turn yield shorter breakthrough times when eompared to ammonia. Further investigation detailing the meehanism of adsorption for eaeh of these eases is necessary and falls beyond the seope of this work.

As with ammonia, breakthrough studies were also conducted at 80% RH, and the results are illustrated in Figure 10.

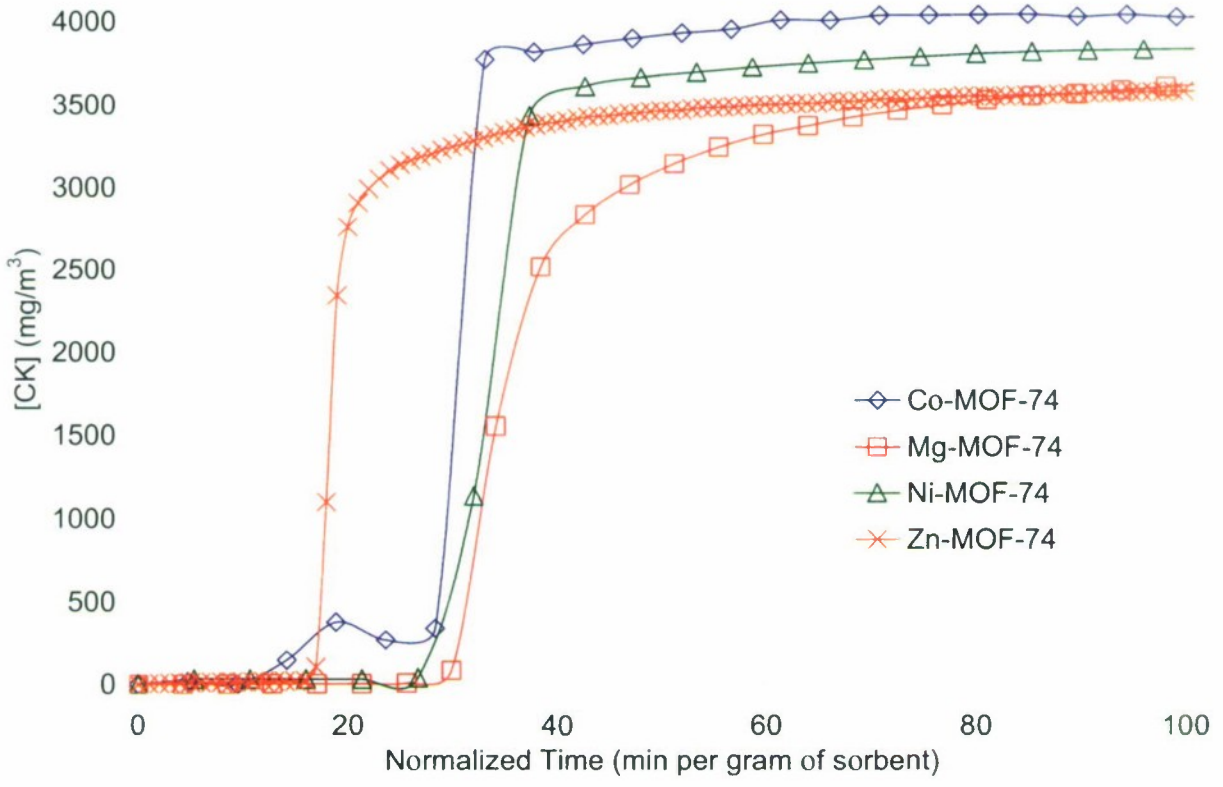

Figure 10. CK breakthrough curves under humid (RH = 80%) conditions

The breakthrough results effectively show no dynamic capaeity filtration of CK by MOF-74 under humid eonditions. From these experiments, it is reasonable to assume that water aggressively competes for adsorption sites with CK on the MOF surfaee. It is also possible that water may more readily eluster in the pore as an adsorbed phase eompared to CK,

given that the vapor pressure of CK at 25 °C is approximately 1200 torr compared to 24 torr vapor pressure of water. As with the ammonia breakthrough studies, the prehumidification of the sample could have also allowed water to occupy nearly all of the available active sites in the MOF structure, or destroyed the MOF porosity, thus preventing CK adsorption. The adsorption results are tabulated in Table 4.

Table 4. CK Dynamic Capacity of Sorbents

MOF-74 Analog	Sorbent Mass*	Effective Loading	Effective Loading (w/Desorption)
	g	mol/kg	mol/kg
Co (Dry)	0.0137	5.640	3.940
Co (Wet)	0.0113	0.047	0.032
Mg (Dry)	0.0136	1.220	0.475
Mg (Wet)	0.0125	0.079	0.027
Ni (Dry)	0.010	2.400	1.830
Ni (Wet)	0.010	0.168	0.123
Zn (Dry)	0.0101	3.580	3.090
Zn (Wet)	0.0134	0.101	0.081

*Dry basis - does not include mass of loaded water

4.1.3 Octane

Octane micro-breakthrough testing was conducted on MOF samples under dry and humid conditions to assess the physical adsorption capacity of MOF-74 materials for hydrocarbons and materials with low vapor pressures.

The results of dry breakthrough experiments for octane are shown in Figure 11. None of these materials offer significant filtration capabilities for the adsorption of octane in dry air as seen by the emergence of the toe of the breakthrough curve in very short times. All of the materials show consistent performance in regards to breakthrough time with the exception of the Co-MOF-74 material. It is possible that the Co-MOF-74 experiment exhibited some channeling behavior as a result of using such small quantities of material.

It is interesting that octane shows no particular preference to the metal in the SBU of the material. One possible explanation is that octane is not complexing with the metals and is rather physisorbing in the pores of the material; thus, only the pore structure of the material makes a contribution to the adsorption capacity.

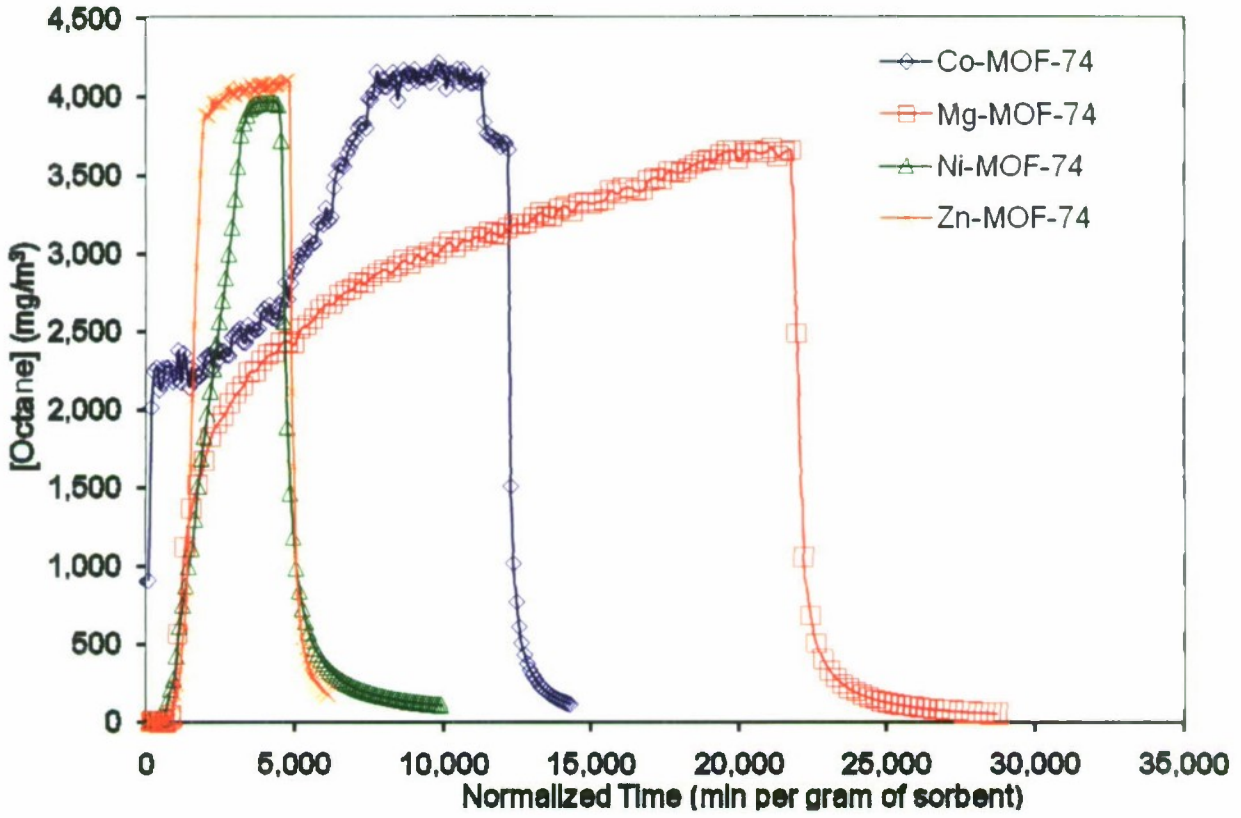

Figure 11. Octane breakthrough curves under dry (RH = 0%) conditions

Under humid conditions, octane breaks through the bed almost immediately as seen in Figure 12. These results are consistent, given the prehumidification of the sample prior to analysis. The water easily adsorbs on the pore structure, and octane is then unable to penetrate the pore structure, most likely due to its limited miscibility in water and its failure to form strong complexes with the metals in the SBU. The dynamic loadings of octane on MOF-74 are shown in Table 5.

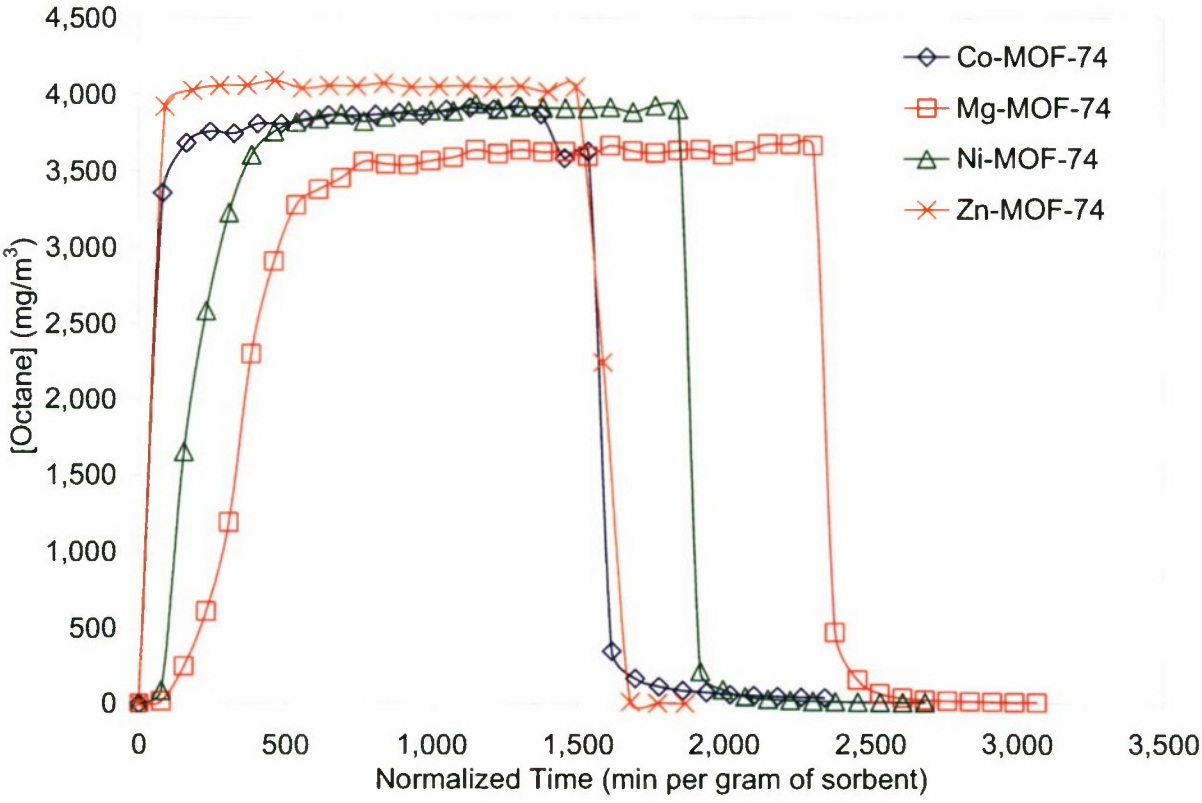

Figure 12. Octane breakthrough curves under humid (RH = 80%) conditions

Table 5. Octane Dynamic Capacity of Sorbents

MOF-74 Analog	Sorbent Mass*	Effective Loading	Effective Loading (w/Desorption)
	g	mol/kg	mol/kg
Co (Dry)	0.0118	1.940	1.220
Co (Wet)	0.0132	0.046	0.000
Mg (Dry)	0.0049	3.480	2.970
Mg (Wet)	0.0217	0.180	0.170
Ni (Dry)	0.0103	1.430	1.030
Ni (Wet)	0.0139	0.160	0.140
Zn (Dry)	0.0156	1.160	1.040
Zn (Wet)	0.0114	0.047	0.031

4.1.4 Sulfur Dioxide

The results of micro-breakthrough experiments with MOF-74 and dry sulfur dioxide are shown in Figure 13. It is clear from the figure that Mg-MOF-74 appears to provide the greatest filtration capability. The Mg-MOF-74 desorption is not shown in Figure 13 to ensure that the curves for the other analogs can be seen at an appropriate scale. The Mg-MOF-74 sample and the other materials all show some reversibility of sulfur dioxide adsorption. The dynamic loadings of sulfur dioxide in these materials are provided in Table 6.

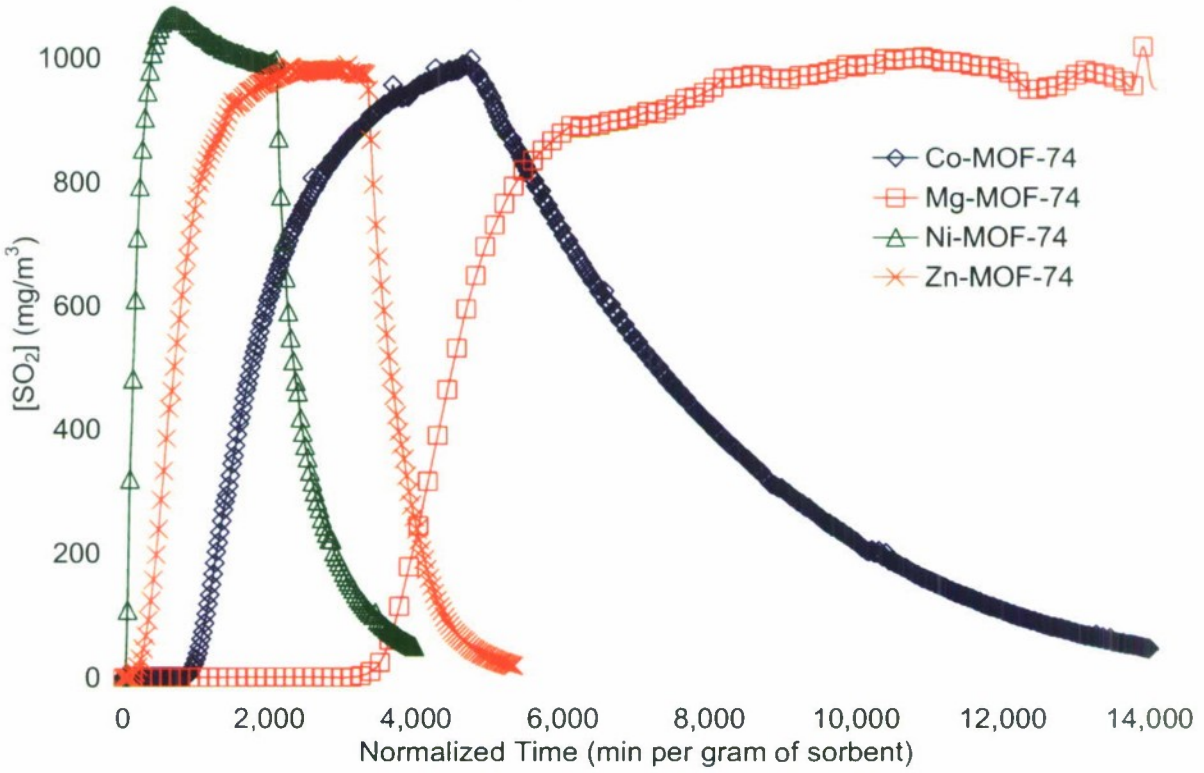

Figure 13. Sulfur Dioxide breakthrough curves under dry (RH = 0%) conditions

The results of humid sulfur dioxide breakthrough experiments are shown in Figure 14. Under humid conditions the Mg-MOF-74 material continues to perform well; however, all of the other MOF-74 analogs effectively lose all of their filtration capacity for sulfur dioxide.

It is also interesting that upon termination of the feed, the Mg-MOF-74 material does not desorb the filtered sulfur dioxide. It is possible that under humid conditions, water coadsorbs with sulfur dioxide, given the polarity of the species; however, polarity and solubility would also apply to the other MOF analogs. Therefore, in this case, it is reasonable to assume that complexes of sulfur dioxide and magnesium are significantly stronger than those formed with other metal SBUs. It is also possible that the SO_2 is either being oxidized to H_2SO_4 or forming a complex similar to $MgSO_4$. Work has also documented the strong preference of magnesium cations for water and oxygen-containing compounds [20], which may explain the

preference of Mg-MOF-74 for SO2 compared to other MOF analogs. The preference of Mg cations for water could also explain why Mg-MOF-74 shows a reduction in its SO_2 capacity under humid conditions.

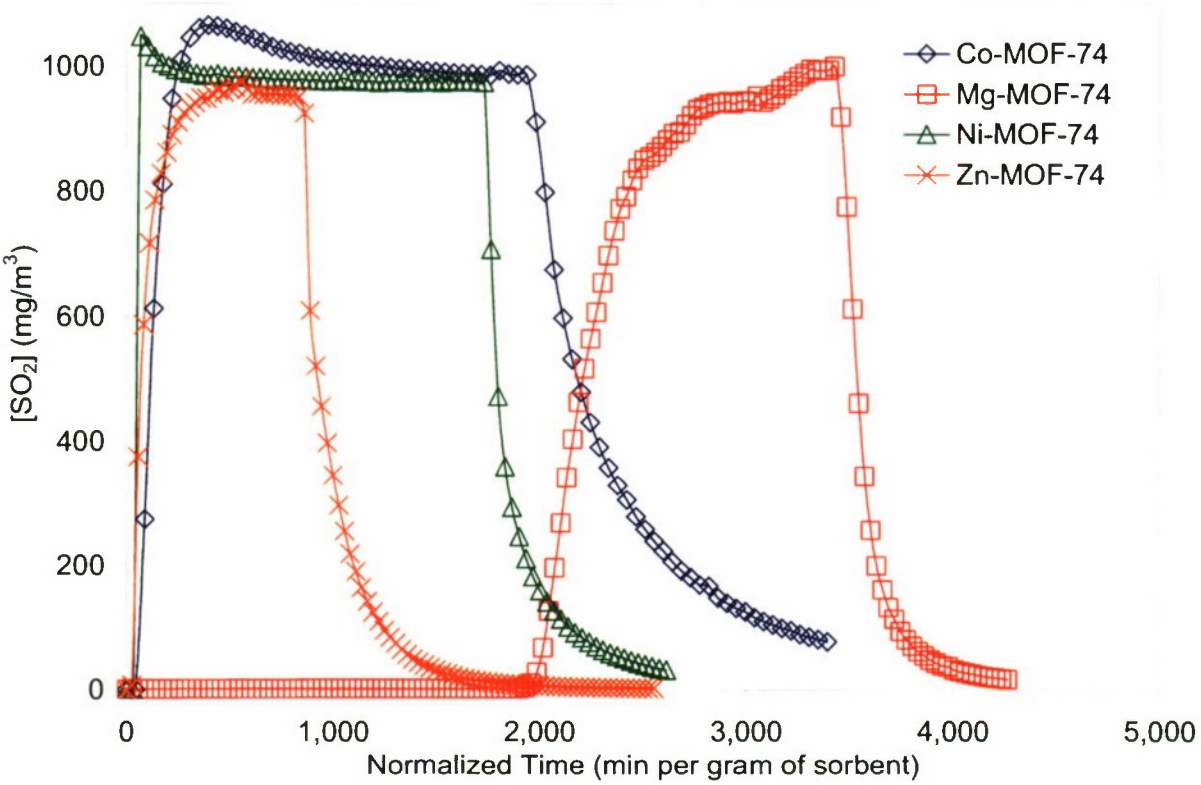

Figure 14. Sulfur dioxide breakthrough curves under humid (RH = 80%) conditions

Table 6. Sulfur Dioxide Dynamic Capacity of Sorbents

MOF-74 Analog	Sorbent Mass*	Effective Loading	Effective Loading (w/Desorption)
	g	mol/kg	mol/kg
Co (Dry)	0.0229	0.627	0.000
Co (Wet)	0.0121	0.032	0.000
Mg (Dry)	0.0041	1.560	0.000
Mg (Wet)	0.0185	0.716	0.669
Ni (Dry)	0.0161	0.035	0.000
Ni (Wet)	0.0157	0.020	0.000
Zn (Dry)	0.0153	0.256	0.121
Zn (Wet)	0.0192	0.039	0.000

*Dry basis - does not include mass of loaded water

4.2 Discussion

A summary of the results discussed above are tabulated in Table 7, where loadings do not reflect desorption. It is clear that magnesium and cobalt perform better than the nickel and zinc analogs of these materials in dry conditions, with the adsorption of CK by Mg-MOF-74 being the only exception. Zinc and nickel MOF-74 materials both behave similarly, each making limited contributions to the adsorption of gases in MOF-74 materials.

It should be noted that these materials were stored in air during the breakthrough testing to be consistent with the second objective of this work, which is the evaluation of MOF-74 analogs as adsorbent media for air purification. By storing the materials in ambient conditions, the breakthrough results provide a more accurate reflection of how these materials would perform as air filtration media.

Under humid conditions, all of the materials show a significant reduction in adsorption capacity. The role of water on the adsorption of these gases in MOF-74 materials is a complex problem involving adsorbent and adsorbate interactions and falls somewhat beyond the scope of this work. It is reasonable to conclude from the breakthrough data that once water is introduced onto the surface of MOF-74, the adsorption capacity of MOF-74 for the gases studied is effectively eliminated. The exception to this is ammonia, which takes advantage of its solubility in water, and the adsorption of sulfur dioxide on Mg-MOF-74.

Breakthrough data do not provide specific knowledge of the mechanism of water adsorption on MOF-74 materials; however, it is likely that the water forms initially as clusters around the metal in the SBU of MOF-74, and these clusters act to seed subsequent adsorption. If it is assumed that the metal in the SBU is the most active adsorption site, then the seeding of water competes for this adsorption surface; thus, the breakthrough times are reduced and total capacity is diminished. Adsorption around the metal site would be consistent with previous work done on MOF-74 materials detailing the adsorption of hydrogen as well as work done detailing the adsorption of nitrogen on other MOFs [16,21].

In addition, it is difficult to speculate how high RH alters the structure of the material. However, because the MOF-74 materials are prehumidified for 2 hr prior to performing the breakthrough tests, it is reasonable that any significant changes to the structure of MOF-74 analogs would have been introduced prior to gathering the breakthrough data.

The breakthrough results do highlight the importance of understanding the formation of complexes of these metals. For example, a material such as octane, which most likely interacts solely with the pore volume of the material in a physisorption process, exhibits limited loading on nearly all of these materials. In the case of octane, the large size of the molecule helps compensate for the lack of complexation through physisorption. However, ammonia, which is significantly smaller than octane, is a strong Lewis base and readily adsorbs on these materials most likely in the formation of metal complexes. Likewise, given that CK and ammonia both posses a lone pair, it is possible that CK and ammonia both exhibit similar complexing and possible adsorption mechanisms. It is also reasonable that CK could be interacting with the SBU via pie-bonding.

Some of the dynamic loadings of the MOF-74 materials are noteworthy. For example, the loading of ammonia on magnesium and cobalt, and the loadings of CK on the cobalt and zinc analogs, are significant. Also, although it is difficult to fully deconvolute all of the parameters in these tests. It is clear that given an isostructural environment, the metal in the SBU will impact the dynamic filtration capacity of the sorbent. The impact could result from structural changes that occur upon exposure to either air or moisture, or it could be that no structural changes are occurring, and all of the differences in the dynamic capacity of these materials are resulting from the metal in the SBU. In either case, the metal is the only variable in these experiments; thus, changes in dynamic loading, as well as the materials structural stability, can be attributed to the metal in the SBU.

Table 7. Comparison of Sorbents Studied

		Metal Incorporated in MOF-74			
		Co	Mg	Ni	Zn
Ammonia Loading (mol/kg)	Dry	6.66	7.62	2.26	3.70
	Wet	4.27	1.67	1.92	2.84
Cyanogen Chloride Loading (CK) (mol/kg)	Dry	5.64	1.22	2.4	3.59
	Wet	0.047	0.079	0.170	0.100
Octane Loading (mol/kg)	Dry	1.94	3.48	1.43	1.16
	Wet	0.046	0.180	0.160	0.048
Sulfur Dioxide Loading (mol/kg)	Dry	0.627	1.56	0.035	0.256
	Wet	0.032	0.716	0.020	0.039

The strong impact of the metal in the SBU of these materials underscores the subtle nanoscale control that is possible via reticular chemistry. In this study, by only altering one structural component of material, it was possible to produce significantly different dynamic loadings. This is best seen in the loading of CK on the cobalt and magnesium analogs and the loading of ammonia on the magnesium and nickel analogs.

In addition, by developing an understanding of the complexes that are possible between a targeted adsorbate and the metal contained in the SBU of the MOF adsorbent, it is possible to envision selecting particular metals and particular isostructual environments to promote strong irreversible adsorption or reaction. The results presented here illustrate these concepts and document why MOFs are particularly appealing for the design of adsorbent materials targeted to remove TIC materials.

5. CONCLUSIONS

Metal-organic framework (MOF-74) presents a unique opportunity to study the effects of metals in an isostructural environment. To investigate the effects of particular metals' structural building units (SBUs) and their impact on the performance of MOF-74 as an adsorbent for air purification, several breakthrough tests of a variety of toxic industrial chemical (TIC) materials were conducted. Of the gases studied, the dry breakthrough results show that these

materials are able to filter ammonia and CK reasonably well. The filtration capacity of these materials for these particular TICs appears to be related to the capability of the TICs to form complexes with the metals in the SBUs.

With the exception of ammonia, and the adsorption of sulfur dioxide on Mg-MOF-74, none of the MOF-74 materials have any capacity for the gases examined in humid conditions. It appears that water competes for the adsorption site and limits the capacity of the material.

The results show that it is possible to introduce significant performance differences into isostructural MOFs by simply changing the metal contained in the SBU. Some of these changes are reflected in the breakthrough times and dynamic loadings reported in this report. Other effects, such as structural stability and sensitivity to moisture, may also be reflected. The results not only illustrate the potential of MOF materials to separate toxic gases from air, but also document the versatility of reticular chemistry in the design of nanoporous materials.

Blank

LITERATURE CITED

1. Yaghi O. M.; O'Keeffe M.; Ockwigh N. W.; Chae H. K.; Eddaoudi M.; Kim J. "Reticular Synthesis and the Design of New Materials." *Nature*, 2003, 423, 705-714.

2. Horike S.; Dinca M.; Tamaki K.; Long J. R. "Size-Selective Lewis Acid Catalysis in a Microporous Metal-Organic Framework with Exposed Mn2+ Coordination Sites." *J. Am. Chem. Soc.*, 2008, 130, 5854-5855.

3. Millward A.; Yaghi O. M. "Metal-Organic Frameworks with Exceptionally High Capacity for Storage of Carbon Dioxide at Room Temperature." *J. Am. Chem. Soc.*, 2005, 127, 17998-17999.

4. Britt D.; Tranchemontagne D.; Yaghi O. M. "Metal-Organic Frameworks with High Capacity and Selectivity for Harmful Gases." *Proc. Nat. Acad. Sci.*, 2008, 105, 11623-11627.

5. Wong-Foy A. G.; Matzger A. J.; Yaghi O. M. "Exceptional H_2 Saturation Uptake in Microporous Metal-Organic Frameworks." *J. Am. Chem. Soc.*, 2006, 128, 3494-3495.

6. Duren T.; Sarkisov L.; Yaghi O. M.; Snurr R. Q. "Design of New Materials for Methane Storage." *Langmuir*, 2004, 20, 2686-2689.

7. B Britt D.; Tranchemontagne D.; Yaghi O. M. "Metal-Organic Frameworks with High Capacity and Selectivity for Harmful Gases." *Proc. Nat. Acad. Sci.*, 2008, 105, 11623-11627.

8. Dathe H.; Peringer E.; Roberst V.; Jentys A.; Lercher J.A. "Metalorganic Frameworks Based on Cu2+ and Benzene-1,3,5-tricarboxylate as Host for SO_2 Trapping Agents." *Comptes Rendus Chimie.*, 2005, 8, 753-763.

9. Dathe H.; Jentys A.; Jercher J. "Sulfate Formation on SO_2 Trapping Materials Studied by Cu- and S-K edge XAFS." *Phys. Chem. Chem. Phys.*, 2005, 7, 1283-1292.

10. Chui S. S. Y.; Lo S. M. F.; Charmant J. P. H.; Orpen A. G.; Williams I. D. "A Chemically Functionalizable Nanoporous Material $[Cu_3(TMA)_2(H_2O_3]_n$." *Science*, 1999, 283, 1148-1150.

11. Rosi N. L.; Kim J.; Eddaoudi M.; Chen B.; O'Keeffe M.; Yaghi O. M. "Rod Packings and Metal-Organic Frameworks Constructed from Rod-Shaped Secondary Building Units." *J. Am. Chem. Soc.*, 2005, 127, 1504-1518.

12. Zhou W.; Wu H.; Yildirim T. "Enhanced H Adsorption in Isostructural Metal-Organic Frameworks with Open Metal Sites: Strong Dependence of the Binding Strength on Metal Ions." *J. Am. Chem. Soc.*, 2008, 130, 15268-15269.

13. Wu H.; Zhou W.; Yildirim T. "High-Capacity Methane Storage in Metal-Organic Frameworks M_2(dhtp): The Important Role of Open Metal Sites." *J. Am. Chem. Soc.*, 2009, 131, 4995-5000.

14. Caskey S. R.; Wong-Foy A. G.; Matzger A. J. "Dramatic Tuning of Carbon Dioxide Uptake via Metal Substitution in a Coordination Polymer with Cylindrical Pores." *J. Am. Chem. Soc.*, 2008, 130, 10870-10871.

15. Vitillo J. G.; Regli L.; Chavan S.; Ricchiardi G.; Spoto G.; Dietzel P. D. C.; Bordiga S.; Zecchina A. "Role of Exposed Metal Sites in Hydrogen Storage in MOFs." *J. Am. Chem. Soc.*, 2008, 130, 8386-8396.

16. Liu Y; Kabbour H.; Brown C. M.; Neumann D. A.; Ahn C. C. "Increasing the Density of Adsorbed Hydrogen with Coordinatively Unsaturated Metal Centers in Metal-Organic Frameworks." *Langmuir*, 2008, 24, 4772-4777.

17. Rudisill E. N.; Hacskaylo J. J.; LeVan M. D. "Coadsorption of Hydrocarbons and Water on BPL Activated Carbon." *Ind. Eng. Chem. Res.*, 1992, 31, 1122-1130.

18. Qi N.; Appel W. S.; LeVan M. D. "Adsorption Dynamics of Organic Compounds and Water Vapor in Activated Carbon." *Ind. Eng. Chem. Res.*, 2006, 45, 2303-2314.

19. Glover T. G.; Wang Y.; LeVan M. D. "Diffusion of Condensable Vapors in Single Adsorbent Particles Measured via Concentration-Swing Frequency Response." *Langmuir*, 2008, 24, 13406-13413.

20. Bock C. W.; Kaufman A.; Glusker J. P. "Coordination of Water to Magnesium Cations." *Inorg. Chem.*, 1994, 33, 419-427.

21. Walton K. S.; Snurr R. Q. "Applicablity of the BET Method for Determining Surface Areas of Microporous Metal-Organic Frameworks." *J. Am. Chem. Soc.*, 2007, 129, 8552-8556.